Sensor Design Using Computer Tools II

John A. Jamieson
Chairman/Editor

Proceedings of SPIE—The International Society for Optical Engineering

Volume 550

Sensor Design Using Computer Tools II

John A. Jamieson
Chairman/Editor

April 11-12, 1985
Arlington, Virginia

Published by
SPIE—The International Society for Optical Engineering
P.O. Box 10, Bellingham, Washington 98227-0010 USA
Telephone 206/676-3290 (Pacific Time) • Telex 46-7053

The papers appearing in this book comprise the proceedings of the meeting mentioned on the cover and title page. They reflect the authors' opinions and are published as presented and without change, in the interests of timely dissemination. Their inclusion in this publication does not necessarily constitute endorsement by the editors or by SPIE.

Please use the following format to cite material from this book:
Author(s), "Title of Paper," *Sensor Design Using Computer Tools II,* John A. Jamieson, Editor, Proc. SPIE 550, page numbers (1985).

Library of Congress Catalog Card No. 85-061487
ISBN 0-89252-585-1

Printed in the United States of America.

SENSOR DESIGN USING COMPUTER TOOLS II

Volume 550

Conference Committee

Chairman
John A. Jamieson
Jamieson Science & Engineering, Incorporated

Session Chairmen
Session 1—Sensor Performance Simulations
Nick G. Gionis, Aerojet ElectroSystems Co.

Session 2—Sensor Subsystem Design and Testing
John Curiale, IBM Corporation

Session 3—Sensor Quality Design and Testing
Phillip E. Howard, Rockwell International Corporation

Session 4—Computers and Professionals
Earle McAuliffe, Boeing Aerospace Company

Panel Discussion—Computers and Professionals
Moderator, **John A. Jamieson,** Jamieson Science & Engineering, Incorporated

SENSOR DESIGN USING COMPUTER TOOLS II

Volume 550

INTRODUCTION

Since the first of these conferences in 1982, the use of computer tools has become more widespread. In the larger aerospace companies, for example, most design engineers are now provided with a personal computer or a terminal at their desks. This trend is changing the way in which engineering work is done, and particularly the amount of optimization of design and automation of testing that is used.

In some kinds of engineering, such as development of semiconductor components and devices, computer tools are becoming duplex links between design and manufacturing; the capabilities of the available manufacturing processes are influencing the designs; the product of the design tools can be used directly to command manufacturing runs. In engineering of whole systems, extensive modeling and simulation of results are being used.

These changes are strongly affecting the work habits and training of engineers. The industry seems to be between a generation of experienced engineers who did not grow up with computers and a younger generation who have not yet acquired the experience to guide application of powerful new tools.

This conference was designed to address the effects of these influences on electro-optical sensor design. Many of the papers were invited. The first session was devoted to sensor performance simulation and modeling. The second session addressed subsystem design and some aspects of process control. The third session was intended to show examples of quality modeling, i.e., reliability, availability and cost modeling; and sensor and subsystem testing. However, in all sessions, but particularly in this one, uncertainties about policies of technology transfer and the difficulty of obtaining written permission to present results caused a number of papers to be withheld or withdrawn. The fourth session was devoted to the effects on professional lives of engineers. It contained a paper on application of personal computers to the imposing task of optimized iterative optical design, an interesting account of the experience of one large aerospace company growing into the new era, and a lively panel session in which representatives of industry and academia—the older generation and the younger—discussed their views in response to prepared questions and questions from the audience.

I wish to express my deep appreciation and gratitude to the authors and to the session chairmen who worked so hard to structure and direct this conference.

John A. Jamieson
Jamieson Science & Engineering, Incorporated

SENSOR DESIGN USING COMPUTER TOOLS II

Volume 550

Contents

SENSOR DESIGN USING COMPUTER TOOLS II

Volume 550

Session 1

Sensor Performance Simulations

Chairman
Nick G. Gionis
Aerojet ElectroSystems Co.

Simulating the performance of imaging sensors for use in realistic tactical environments

Brian K. Matise
Timothy J. Rogne

OptiMetrics, Inc.
2000 Hogback Road, Suite 3, Ann Arbor, Michigan 48104

Grant R. Gerhart
James M. Graziano

U.S. Army Tank-Automotive Command Research and Development Center
Attn: DRSTA-ZSA, Warren, Michigan 48090

Abstract

An imaging sensor simulation model is described which allows a modeled or measured scene radiance map to be displayed on a video monitor as it would be seen if viewed through a simulated sensor under simulated environmental conditions. The model includes atmospheric effects (transmittance, path radiance, and single-scattered solar radiance) by incorporating a modified version of the LOWTRAN 6 code. Obscuration and scattered radiance introduced into the scene by battlefield induced contaminants are represented by a battlefield effects module. This module treats smoke clouds as a series of Gaussian puffs whose transport and diffusion are modeled in a semi-random fashion to simulate atmospheric turbulence.

The imaging sensor is modeled by rigorous application of appropriate optical transfer functions with appropriate insertion of random system noise. The simulation includes atmospheric turbulence transfer functions according to the method of Fried. Of particular use to sensor designers, the various effects may be applied individually or in sequence to observe which effects are responsible for image distortion. Sensor parameters may be modified interactively, or recalled from a sensor library. The range of the sensor from a measured scene may be varied in the simulation, and background and target radiance maps may be combined into a single image.

The computer model itself is written in FORTRAN IV so that it may be transported between a wide variety of computer installations. Currently, versions of the model are running on a VAX 11/750 and an Amdahl 5860. The model is menu driven allowing for convenient operation. The model has been designed to output processed images to a COMTAL image processing system for observer interpretation. Preliminary validation of the simulation using unbiased observer interpretation of minimum resolvable temperature (MRT)-type bar patterns is presented.

Introduction

The performance of electro-optical sensors designed for use in realistic battlefield environments may be difficult to predict due to the complexities involved in modeling the scenario. In particular, the performance of imaging sensors which are designed for use by trained human observers may depend on the ability of the sensor to preserve and the observer to detect certain cue features which are present in the scene. The effects of complex backgrounds, the intervening atmosphere, and spatially inhomogeneous obscuration from battlefield-induced contaminants may also affect target recognition. The option of field testing each sensor in a tactical environment is usually unacceptable due to the burdens of creating a sufficient number of representative scenarios and necessity of constructing a prototype sensor.

An imaging sensor simulation which maintains the trained human observer in the image interpretation process overcomes the principal modeling difficulty while permitting flexibility in reproducing scenarios.

Structure of the simulation

The simulation requires a scene radiance map at some known location from the sensor as an input. The map may be either a measured scene radiance map, a combination of measured backgrounds or targets, or a modeled radiance map. If the input map is obtained by a sensor which introduces distortions which are not negligible, or is obtained at a range which is sufficiently large so that the intervening atmosphere will introduce significant effects, the simulation attempts to remove these effects by inverse application of the atmospheric effects and sensor effects algorithms. The ability of the simulation to remove these effects is limited by the noise in the measured data and the accuracy to which the sensor effects and environmental effects may be represented.

Three separate modules act on the scene radiance map. These modules incorporate the effects of spatially homogeneous obscuration due to the natural atmosphere, spatially inhomogeneous obscuration due to screening smokes and other battlefield induced contaminants, and image degradation introduced by the viewing sensor. Each of these modules is based on a separate and complete physical model.

The resulting sensor voltage map may be displayed by an observer on a video monitor. Gain and level adjustments are provided so that the observer may adjust the dynamic range of the displayed image as would be permitted with an actual sensor.

Natural atmospheric effects module

Atmospheric transmittance and radiance are incorporated into the scene radiance map through calculations performed by a modified version of LOWTRAN 6.[1] This code is a moderate resolution (20 cm^{-1}) band model which includes standard atmospheric profiles, aerosol models, and molecular absorption parameters for wavelengths from 250 nm to 28.5 μm.

The effects of the natural atmosphere which are treated in the simulation include absorption by atmospheric gases, molecular scattering, absorption and scattering by haze and fog aerosols, and absorption and scattering due to rain. Path radiance which is added to the transmitted radiance includes emission and single scattered solar radiation. Specifically excluded from consideration are multiply scattered photons, atmospheric emissions scattered into the path of interest, and radiation scattered from extended sources such as the ground.

The version of LOWTRAN 6 which is incorporated in the simulation has been modified to include only those scenarios relevant to ground vehicle signature applications. This has enabled the set of required inputs to be reduced considerably.

The simulation currently treats obscuration due to the natural atmosphere as homogeneous across the scene and dependent only on range. Band-averaged values for transmittance and path radiance are applied to each element in the scene radiance map based on

$$L_a(x,y) = L_p + L_s(x,y)\ \tau \qquad (1)$$

where L_a = apparent scene radiance map
L_p = natural atmosphere path radiance
L_s = scene radiance map
τ = natural atmosphere transmittance

Battlefield effects module

Imaging sensors intended for tactical battlefield applications must be designed with the knowledge that spatially inhomogeneous obscuration due to intentionally deployed smokes and inadvertent battlefield induced contaminants may be present. Such obscuration may affect sensor performance depending on the characteristics of the sensor, the sensor-target-obscurant geometry, meteorological conditions, and obscurant characteristics. The effects of this obscuration may be difficult to predict without simulating specific scenarios.

The imaging sensor simulation model incorporates the effects of battlefield obscurants by means of the ACTMAD battlefield effects model[2]. This model was developed by OptiMetrics under contract to the US Army Atmospheric Sciences Laboratory (ASL) as a derivative of the ASL code, ACT II[3]. Transport and diffusion of smoke clouds may be modeled by either a Gaussian plume methodology or a semi-random microscale atmospheric dispersion of Gaussian puffs methodology. The latter approach permits the spatial and temporal inhomogeneities in the smoke cloud to be modeled in a deterministic manner.

The battlefield effects module currently contains default characteristics for two varieties of vehicle self-screening smoke grenades. However, virtually any type of smoke source may be included in the model if the user provides the appropriate source parameters. Obscuration effects considered include extinction, path emission, smoke emissions scattered into the line of sight, solar radiation scattered into the path, and radiation from the sky-ground sphere scattered into the path.

The obscuration effects of the battlefield module are incorporated into the scene radiance map in the following manner:

$$L_a(x,y) = L_{p2} + L_{ps}(x,y)\tau_{a2} + L_{p1}\tau_{a2}\tau_s(x,y) + L_s(x,y)\tau_{a2}\tau_s(x,y)\tau_{a1} \quad (2)$$

where L_a = apparent scene radiance map
$L_{p1,2}$ = natural atmosphere path radiance from target-smoke cloud and smoke cloud-observer path segments, respectively
$\tau_{a1,2}$ = natural atmosphere transmittance along target-smoke cloud and smoke cloud-observer path segments, respectively
τ_s = obscurant transmittance map
L_{ps} = obscurant path radiance map
L_s = scene radiance map

The geometry of the scene radiance map plane, smoke event, and sensor is specified by the user by means of a reference coordinate system, in which the sensor location, smoke munition placement, and termination of a single line of sight to the target plane are specified. The coordinate system definition and smoke munition placement, along with necessary meteorological and source characteristics, may be defined by the user prior to run time as part of an input library of smoke scenarios. The spatial resolution at which rigorous calculations through the smoke cloud are performed may be varied by the user at run time to minimize the computational load while retaining realism. Each pixel in the scene radiance map is then modified based on a linear interpolation of the transmittance and path radiance in the calculation grid.

Sensor module

The sensor module accepts an input radiance map, as modified by natural or battlefield environment effects, which is converted to a map of optical power received by the detector from each scene element. This signal map is then Fourier transformed so that linear optical transfer functions representing the effect of sensor subsystems may be conveniently applied.

The linear optical transfer functions utilized by the sensor model are based on the subsystem transfer function forms included in the NV&EOL Static Performance Model for Thermal Viewing Systems[4]. The most notable exceptions are that display and observer effects are simulated rather than modeled. Table 1 lists the set of pre-defined subsystem transfer functions. In addition to the transfer functions defined in the table, the user may define tabular modulation transfer functions to be used in the sensor definition.

Table 1. Sensor Subsystem Transfer Function Definitions

Optics - Diffraction

$$H(k_x,k_y) = \frac{2}{\pi}\left[\cos^{-1}(A) - A(1-A^2)^{1/2}\right]$$

$$A = \lambda_D(f/\#)\,k_{xy}/F$$

$$k_{xy} = (k_x^2 + k_y^2)^{1/2}$$

λ_D = diffraction wavelength (microns)
$f/\#$ = optical system f - number
k_x = spatial frequency in the along-scan dimension ($mrad^{-1}$)
k_y = spatial frequency in the cross-scan dimension ($mrad^{-1}$)
F = optical system focal length (millimeters)

Optics - Blur

$$H(k_x,k_y) = e^{-b(k_x^2+k_y^2)}$$

$b = \pi^2 w^2$
$w = e^{-1}$ half-width of the optical system point spread function (mrad)

Table 1. (continued)

Atmospheric Turbulence

$$H(k_x,k_y) = e^{-3.44\left(\frac{\lambda_D k_{xy}}{1000\ R_0}\right)^{5/3}\left[1.0-0.5\left(\frac{\lambda_D k_{xy}}{1000\ D}\right)^{1/3}\right]}$$

R_0 = atmospheric coherence length (m)

$$= \left[0.159\ C_n^2\left(\frac{2\pi}{10^{-6}\ \lambda_D}\right)^2 r\right]^{-0.6}$$

D = optical system aperture diameter (m)
C_n^2 = refractive index structure parameter ($m^{-2/3}$)
r = sensor-target range (m)

Detector - Temporal Transfer Function

$$H(k_x) = \frac{1.0}{1.0 + j\left(\frac{k_x v}{f_D}\right)}$$

$$v = \frac{FOV_x\ FOV_y\ F_r\ \eta_{ov}}{n_p\ IFOV_y\ \eta_{sc}}$$

v = scan velocity (mrad/s)
FOV_x = sensor along-scan field-of-view (mrad)
FOV_y = sensor cross-scan field-of-view (mrad)
F_r = frame rate (s^{-1})
η_{ov} = overscan ratio
n_p = number of detectors in parallel
$IFOV_y$ = sensor instantaneous field-of-view in the cross-scan direction (mrad)
η_{sc} = scan efficiency

Detector-Spatial Transfer Function

$$H(k_x,k_y) = \text{sinc}(\pi\ IFOV_x k_x)\ \text{sinc}(\pi\ IFOV_y\ k_y)$$

$IFOV_x$ = sensor instantaneous field-of-view in the along-scan direction (mrad)
$\text{sinc}(x)$ = $\sin(x)/x$

Electronics

$$H(k_x) = \left[\frac{1.0}{1.0 + j\left(\frac{k_x v}{f_{LP}}\right)}\right]\left[\frac{j\ \frac{k_x v}{f_{HP}}}{1 + j\left(\frac{k_x v}{f_{HP}}\right)}\right]$$

f_{LP} = electronics cut-off frequency (Hz)
f_{HP} = electronics cut-on frequency (Hz)

Electronic Boost

$$H(k_x) = 1.0 + \frac{(B-1.0)}{2.0}\left(1.0 - \cos\ \frac{\pi\ v\ k_x}{f_{max}}\right)$$

f_{max} = frequency of maximum boost (Hz)
B = boost at frequency f_{max}

LEDs

$$H(k_x,k_y) = \text{sinc}(\pi\ LED_x\ k_x)\ \text{sinc}(\pi\ LED_y\ k_y)$$

Table 1.- (continued)

LED_x = along-scan LED dimension (mrad)
LED_y = cross-scan LED dimension (mrad)

Sampling

$$H(k_x) = \mathrm{sinc}\left(\frac{\pi v k_x}{2 f_{nyq}}\right) e^{-j\left(\frac{\pi v k_x}{2 f_{nyq}}\right)}$$

f_{nyq} = Nyquist frequency determined by the sampling rate (Hz)

Stabilization

$$H(k_x, k_y) = e^{-\left(S_x k_x^2\right)} e^{-\left(S_y k_y^2\right)}$$

S_x = along-scan stabilization parameter ($mrad^2$)
S_y = cross-scan stabilization parameter ($mrad^2$)

The sensor model allows noise to be added to the signal in the frequency domain at a point just following the system detector(s). All sensor subsystems following the detector then act on both the signal and the noise. Adding the noise in the frequency domain allows any arbitrary noise power spectrum to be easily represented. To represent a white noise spectrum in the frequency domain, the power spectral density is given by

$$\Phi_n = A_d / n_s \, (F_r \, T_e) \, (D^*)^2 \qquad (3)$$

where Φ_n = noise power spectral density (W^2/Hz)
A_d = detector element area (cm^2)
n_s = number of detectors in series
F_r = frame rate (s^{-1})
T_e = eye integration time (s)
D^* = detector peak detectivity ($cm\text{-}(Hz)^{1/2}/W$)

The actual sample of noise which is added to each frequency domain image element is then computed as

$$\mathrm{Noise}_i = (\Phi_n/2)^{1/2} N_k + j \, (\Phi_n/2)^{1/2} N_{k+1} \qquad (4)$$

where Noise_i = noise added to a frequency domain element
N_k = normally distributed random number with zero mean and unit variance

The sensor subsystem transfer functions may be applied individually or in sequence when simulating the performance of a sensor on a given scene radiance map. In this manner, the major contributions to image quality destruction may be observed. The effects of modifying one or more of the sensor's characteristics may also be simulated.

The atmospheric turbulence transfer function we have chosen to incorporate is the near-field formulation of the short exposure case developed by Fried[5]. The effects of turbulence on image quality may be varied by the user by selecting different estimates of the refractive index structure constant, C_n^2.

Image display

The version of the simulation running on the VAX 11/750 system at TACOM is designed to display the image on a COMTAL image processing system. The simulation can process image arrays up to 256x256 pixels and provide 8-bit output resolution. The simulation can also write image arrays to 9-track magnetic tape and produce variable density printer plots.

Simulation output

The performance of the simulation in representing sensor output as range is varied under relatively clear atmospheric conditions is demonstrated in Figure 1. The measured scene radiance map used as the input for all sensor simulations described below is that of an M-60 tank parked in an open field (Figure 1a). The sensor we are simulating in Figure 1 b-d is a current technology, man-portable thermal imaging sensor. The atmospheric conditions cor-

respond to a midlatitude winter model atmosphere with 23 km visibility. Note that we have essentially zoomed the simulated display range so that the apparent target size does not change with range. The simulation has also automatically self-scaled the display contrast and brightness to maximize the dynamic range. This option can be disabled if the user enters a range of apparent radiances to be displayed.

In Figure 2 we compare the scene appearance as viewed through three different simulated sensors. Sensor A is a current-technology, man-portable system using N detectors; sensor B is the same system using 2N detectors. Sensor C is a high-resolution, airborne system. The simulated range in Figure 2 is 1 km, with visibility limited to 2 km by an advection fog.

Figure 3 simulates the output of the battlefield effects module. In this image, obscuration due to infrared screening grenades 2 seconds after dissemination has been added to the original scene radiance map. The variation in brightness across the smoke cloud is due to the reflection of varying amounts of sky radiance into the line of sight.

Model validation

Preliminary validation of the sensor model consisted of predicting the minimum resolvable temperature (MRT) characteristic of an existing sensor for which both measured data and detailed modeling information exist. The sensor we have modeled is a pre-production version of the Target Acquisition Designation System (TADS) thermal imaging sensor. Reference 6 provides measured data and NVL static performance model inputs which describe the sensor.

The simulation modeled the sensor viewing a standard 4-bar MRT target presented against a uniform background. We ran the simulation for a matrix of cases which included a number of different target contrast signature levels for each of 5 different bar pattern spatial frequencies. The resulting set of images was then viewed individually by each of 9 observers. The observers were allowed to optimize the display contrast of each image and adjust their viewing position in any way they desired, as would be permitted observers in a real MRT test. Within each set of images at a particular spatial frequency, the observers were asked to select the lowest contrast signature image in which they could both detect and resolve the MRT pattern. Typical bar pattern images are displayed in Figure 4.

The results of this test are summarized in Table 2. The results are presented as the ratio of the MRT obtained by the observers viewing the simulation to the measured system MRT. The ratio of the MRT predicted by the NVL static performance model to the measured system MRT is also presented for comparison. Note that there is a variation among the observers at all spatial frequencies except the lowest. Interestingly, the predictions based on observer responses compare very favorably with the measured data, with predictions made using the NVL model directly showing relatively less agreement. However, while the results of this preliminary test are certainly interesting, they cannot be considered a sufficient basis for drawing any conclusions.

Table 2. Minimum Resolvable Temperature (MRT) Simulation Test Results

Spatial Frequency	Ratio of Simulation Observer MRTs to Measured System MRT: Simulation Observer MRTs (K) 1	2	3	4	5	6	7	8	9	Ratio of Observer Average MRT to Measured System MRT	Ratio of NVL Predicted MRT to Measured System MRT
0.125 F_o*	4.8	4.8	4.8	4.8	4.8	4.8	4.8	4.8	4.8*	4.8*	---**
0.37 F_o	1.1	0.8	0.8	1.1	1.1	0.8	1.1	0.8	1.1	0.936	0.253
0.46 F_o	1.0	0.7	0.8	1.0	1.0	1.0	0.8	0.7	1.2	0.907	0.283
0.56 F_o	0.8	0.8	0.8	1.0	1.0	0.8	0.8	0.8	1.0	0.844	0.481
0.65 F_o	1.1	0.6	0.8	1.1	1.1	1.1	0.8	0.8	0.8	0.910	0.724

* Ratio of observer MRT to NVL predicted MRT.
** Measured system MRT not available.

There has been no attempt to validate the atmospheric and battlefield effects modules by comparison with measured data. Since these modules are based on previous models which have been developed and tested, we have only verified that their performance in the simulation matches the output of the original models.

A thorough field performance validation of the simulation is planned in the coming year. The planned validation effort will involve exercising the simulation to predict long-range forward-looking infrared (FLIR) imagery given an input set which consists of close-range, high resolution target imagery and simultaneously measured meteorological and transmission data.

Acknowledgment

The authors would like to acknowledge the cooperation and support of the US Army Tank-Automotive Command (TACOM) and TACOM personnel in the development of this model. Development of the simulation was performed under Contract DAAE07-81-C-4053. The original imagery which was used as input to the model was obtained as part of the TACOM Standard Scenes Project which is directed by Dr. David Wilburn of TACOM. Dr. Wilburn also served as Principal Technical Representative on Contract DAAE07-81-C-4053.

References

1. Kneizys, F. X., et al. , Atmospheric Transmittance/Radiance: Computer Code LOWTRAN 6, AFGL-TR-83-0187, Air Force Geophysics Laboratory, Hanscom AFB, MA, August 1983.

2. Matise, B. K. et al., Smoke Obscuration Effects Model, OMI-82-025, OptiMetrics, Inc., December 1982.

3. Sutherland, R. A. and Hoock, D. W., An Improved Smoke Obscuration Model ACT II: Part I Theory, ASL-TR-0104, US Army Atmospheric Sciences Laboratory, White Sands Missile Range, NM, January 1982.

4. Ratches, J. A. et al., Night Vision Laboratory Static Performance Model for Thermal Viewing Systems, ECOM-7043, US Army Night Vision and Electro-Optics Laboratory, Ft. Belvoir, VA, April 1975.

5. Fried, D. L., "Optical Resolution through a Randomly Inhomogeneous Medium for Very Long and Very Short Exposures", JOSA, Vol. 56, p. 1372. October 1966.

6. TADS System Specifications, NVL Static Performance Model Input Set, designed to simulate the TADS thermal imager. Supplied to US Army Missile Command by Martin Marietta Corporation in an unpublished document (CONFIDENTIAL).

(a) original image

(b) 1 km range

(c) 3 km range

(d) 5 km range

Figure 1. Simulated displayed imagery for several viewing ranges under clear atmospheric conditions. Sensor B.

(a) Sensor A

(b) Sensor B

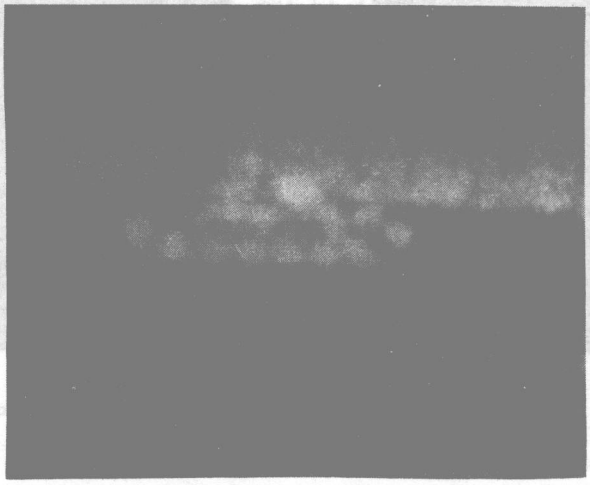

(c) Sensor C

Figure 2. Comparison of three thermal imaging sensors operating at a simulated range of 1 km under 2 km visibility fog conditions.

Figure 3. Simulation of two infrared screening grenades, two seconds after detonation.

(a) $\Delta T = T_o$ (b) $\Delta T = 4T_o$

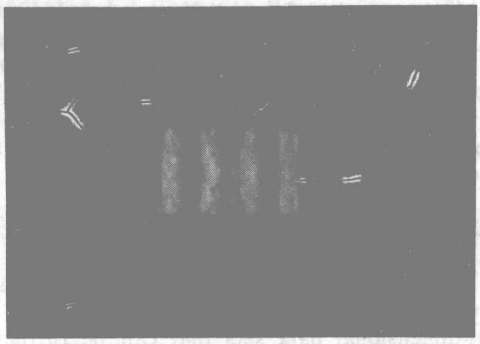

(c) $\Delta T = 6T_o$

Figure 4. Simulated images of a 4-bar MRT target as viewed by a pre-production version of the TADS thermal imaging sensor at three different target contrast signature levels.